

Inkjet 3D Printed MEMS Vibrational Electromagnetic Energy Harvester

Bartosz Kawa ¹, Krzysztof Śliwa ¹, Vincent Ch. Lee ² and Qiongfang Shi ^{2,*}, Rafał Walczak ^{1,*}

¹ Department of Microsystems, Wrocław University of Science and Technology; 50370 Wrocław, Poland; bartosz.kawa@pwr.edu.pl (B.K.); krzysztof.sliwa@pwr.edu.pl (K.Ś.)

² Department of Electrical and Computer Engineering, National University of Singapore, Singapore 117608, Singapore; elelc@nus.edu.sg (V.C.L.); eleshiq@nus.edu.sg (Q.S.)

* Correspondence: rafal.walczak@pwr.edu.pl; Tel.: +48-320-4973

Received: 6 May 2020; Accepted: 1 June 2020; Published: 1 June 2020

Abstract: Three-dimensional (3D) printing is a powerful tool that enables the printing of almost unlimited geometry in a few hours, from a virtual design to a real structure. In this paper, we present a micro-electromechanical energy harvester that utilized a 3D printed micromechanical structure combined with a miniature permanent magnet and a microelectronic coil towards a hybrid electromagnetic vibrational hybrid energy harvester. Various micromechanical structure geometries were designed, printed, and tested. The characteristic dimensions of the springs were from 200 μm to 400 μm and the total volume of the devices was below 1 cm^3 . The resonant frequencies (95–340 Hz range), as well as bandwidths (6–23 Hz range), for the developed prototypes were determined. The maximal generated output power was almost 24 W with a power density up to almost 600 W/cm^3 .

Keywords: 3D printing; MEMS; energy harvester

1. Introduction

Micro-electromechanical systems (MEMS) combine mechanical microstructures with microelectronic circuits to create a very small functional system that senses, actuates, or harvests energy. The technology of the micromechanical structures in MEMSs involves applying many well-known techniques to the specific materials. Silicon and glass are micromachined mainly by wet or dry etching [1–3], polymer microstructures are formed by injection molding, hot embossing, or soft lithography [4–7], and low-temperature co-fired ceramic substrates are cut and co-fired [8]. Regardless of the applied material and technology, the fabrication of MEMSs is a multistep process involving many technological steps (photolithography, etching, deposition, bonding, assembling, etc.) that require specialized facilities (i.e., apparatus and clean rooms), trained staff, and often knowledge on the properties of the applied materials and limits of the used techniques that are collected over years of experience. All these issues mean that although single MEMSs are usually low-cost devices, a further decrease in the cost-per-chip is difficult to achieve. This is important because some of the forecasts from established companies and institutions (including Bosch, HP, Cisco, and Intel) clearly indicate that in the next decade, the number of MEMS-based devices connected to the internet (Internet of Things, IoT) is going to reach the level of trillions [9]. From an economical point of view, this requires a decrease in the cost of networked MEMSs by at least one or two orders of magnitude. A low price and short development time would result in a higher availability of networked MEMSs for the IoT approach. One promising technology that may decrease the fabrication costs of MEMSs is additive manufacturing, commonly known as 3D printing. Various 3D printing techniques (for example, inkjet printing, stereolithography, or fused deposition

modeling) were already successfully applied to develop some MEMS devices. The exponential growth of scientific papers on 3D-printed microfluidic chips is observed during the last decade [10–14]. Additive manufacturing enables the fast and cost-effective development of truly three-dimensional microfluidic structures. Additionally, a boom in 3D printed sensors is widely reported [15]. A discussion on the applicability of inkjet 3D printing in MEMS technology was recently presented by Walczak [16]. In addition, some examples of 3D printed microdevices, including pumps [17], valves [18], flow regulators [19], electrostatic actuators [20], fuze [21], or specialized packages for MEMS devices [22]. Thus, 3D printing seems to be an attractive alternative for standard microengineering techniques applied in MEMS technology.

The energy source for the power supply of MEMS-based sensing nodes in IoT systems is a crucial issue in decreasing the cost. A comprehensive review on MEMS vibrational energy harvesters was recently presented by Toshiyoshi et al. [23]. After years of miniature energy harvester development, more than a few mW of power can be gained for the power supply of low-power electronic circuits using photovoltaic cells or thermoelectric generators. Mechanical vibration is an attractive candidate as an energy source because it is available almost everywhere. Thus, electromagnetic [24], piezoelectric [25], triboelectric [26], or electrostatic [27] MEMS energy harvesters are reported in the literature. Those devices produce electric energy from a few W to a few mW. They are made from traditional materials (silicon glass, polymers, metals) using microelectronic and microengineering techniques related to MEMS technology. Only a few of them are utilizing 3D printing technology as a fabrication tool.

The first reported applications of 3D printing were for the housing of the energy harvester. Due to the required low precision of the housing fabrication, a fused deposition modeling (FDM) technique was applied [28,29]. Ju et al. described an impact-based piezoelectric vibrational energy harvester that had FDM printed housing with $26 \times 10 \times 10 \text{ mm}^3$ dimensions [28]. Maharjan et al. presented a 3D-printed hybridized electromagnetic–triboelectric nanogenerator where two half parts of the housing (circular tubes with a 1.45 cm inner diameter and an outer diameter of a few cm) were 3D printed [29]. The next step in the evolution of 3D-printed energy harvesters was the fabrication of the active mechanical elements of the energy harvesters. Seol et al. described all 3D-printed triboelectric energy harvesters [30]. A grating disk type triboelectric nanogenerator was fabricated by assembling a 3D-printed electrode layer, a triboelectric layer, and a case package. In this solution, three printing techniques—metal printing, FDM, and stereolithography (STL)—were successfully applied. The overall dimensions of the device were counted in cm. The achieved power density was 4.52 mW/cm^3 . The same group of researchers also developed a triboelectric nanogenerator consisting of a 3D-printed case, a core oscillator, and a spring, all printed using the FDM technique. The harvester was 90 mm long, 30 mm wide, and 15 mm high. It produced a maximum voltage of 98.2 V and current of 13.7 μA [31]. Electromagnetic energy harvesters have also been developed with the use of 3D printing. Hadas et al. designed and tested an energy harvester with FDM-printed immovable elements of the device [32]. The dimensions of the harvester were $8 \times 6 \times 6 \text{ cm}^3$ and the maximal generated power was equal to 26 mW (power density 90 W/cm^3). Immovable elements printed using FDM were also successfully applied in the energy harvester developed by Rues et al. [33]. The harvester had the dimensions of $4.5 \times 5.5 \times 4 \text{ cm}^3$, and 127 mW was measured as the maximum possible generated power (power density 1.28 mW/cm^3). Spherical magnetic generators for bio-motional energy harvesting were developed by Bowers et al. [34]. Two semispherical energy harvester structures with a total diameter of 1.91 cm were inkjet printed and glued together. The maximal generated output power was 1.44 mW (power density around 0.4 W/cm^3). A nonlinear vibrational energy harvester was described by Constantinou et al. [35]. The dimensions of the printed harvester were around $6 \times 4 \times 2 \text{ cm}^3$, but the vibrating double beam was 17.8 mm high, with a single beam thickness of 0.8 mm and a width of 4 mm. The maximal generated power density was 0.48 mW/cm^3 . Only in a few of the reports listed above were 3D-printed movable mechanical components coupled with an electromagnetic circuit operating at the resonance of the oscillating mechanism. The dimensions of most of the printed harvesters were in cm, with a volume well above 1 cm^3 . The FDM

technique dominates as the technique for printing mechanical elements due to its simplicity and the low costs of the printing material and device.

In this paper, we demonstrate the use of inkjet 3D printing as a technique that enables the fabrication of micro-electromechanical electromagnetic energy harvesters with a volume below 1 cm³. We consider simple micro-mechanic structures with a seismic mass suspended on springs with different geometrical dimensions. Numerical simulations of the resonance frequencies are followed by measurements. A critical issue is the measurement of the real mechanical properties of the investigated structures as input data for simulations. Finally, the electrical characteristics of the 3D-printed harvesters, as well as the generated power as a function of the vibration frequency and resistive load, are presented and discussed.

2. Materials and Methods

2.1. Design and Numerical Simulations

The harvesters were designed using Inventor software (Autodesk, USA). The external dimensions of the device were the same for all considered internal designs (Figure 1). The internal structure consisted of a seismic mass with a place for small commercial permanent neodymium magnets (1.5 mm in diameter, 1 mm high, Webcraft, Germany). One or two magnets were positioned on the sides of the vibrating microstructure. The seismic mass was suspended on springs (various designs) with thicknesses of 200 μ m or 400 μ m. The internal structure volume, called the active volume [35], was taken into account in the calculation of the generated power density. At a distance of 2 mm above the magnets, a commercially available miniature surface-mounted coil (SMD 812 with 7.36 mH inductance) was positioned in a printed holder. The output voltage from the coil was connected to a measurement setup. The scheme of the harvester and a computer visualization of one of the designed harvesters with a magnet and coil is shown in Figure 1. Simulations of the natural resonance frequency of the vibrating structure with magnets were carried out using Inventor software (Autodesk, USA). The simulations were conducted for an acrylonitrile butadiene styrene-like material with a Young's modulus equal to the printing material's data sheet ($E = 1423$ MPa) and test structures measured by us.

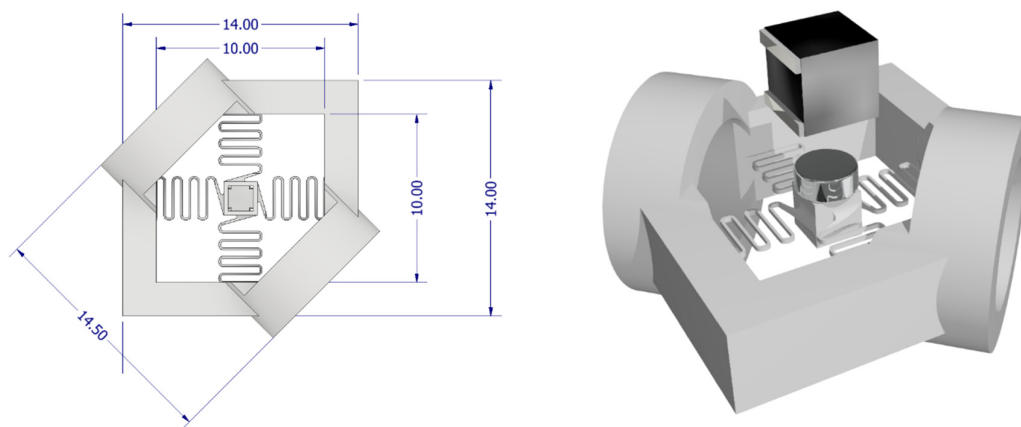


Figure 1. (left) Visualization of the 3D-printed energy harvester with main dimensions in mm and (right) with assembled magnet coupled with one miniature coil.

2.2. Inkjet 3D Printing

The devices were fabricated using inkjet 3D printing. Harvester structures were printed using a 3D Systems ProJet 3510 printer with ultra-high definition resolution (single layer thickness equal to 16 μ m and planar X–Y resolution of 750 dpi). Two standard inkjet printing materials, Visijet M3 Crystal

(as building material) and S300 (as support material), were utilized. The layer structure of the harvester (including the spring structure) was printed parallel to the printing platform. This is an important printing parameter due to the different mechanical properties of microstructures with various layers of internal structure [36,37]. Post-processing was carried out according to a procedure developed by us and described in [38]. Briefly, raw printed structures with support material were put in an oven (2.5 h at 60 °C) to melt away the support material. The structures were cleaned in mineral oil at 60 °C with ultrasonic agitation (1 h). Finally, the structures were rinsed with deionized water and dried in a stream of dry air.

2.3. Determination of Young's Modulus

It is well known from our previous works that printed microstructures with dimensions like those considered in this paper have a different Young's modulus than reported in the material's data sheet. Therefore, knowledge of the real material properties is crucial for simulation parameters. In order to measure the real Young's modulus of the microstructures, ten microbeams with a constant length (6 mm) and 200 µm or 400 µm width and thickness were printed. They were printed in the same process, with the same dimensions, and mechanically characterized. The mechanical characterization of the microbeams was carried out according to the procedure and apparatus applied by us earlier, as described in [37]. The procedure involved a Bondtester Dage 4000 Plus (Nordson Dage, Germany) for microbeam deflection versus applied bending force. The deflection of the microbeam was measured with ± 1 µm accuracy. The maximal deflection was set to 1.25 mm and the maximal applied force was 70 mN (limited by the device settings). In order to investigate the potential aging of the loaded microstructure, the microbeams were deflected 100 times. The values of deflection for the first and last loading tests for 10% and 90% of the maximal applied force were determined and used to calculate Young's modulus according to the following equation (concentrated force at the free end) [37] (1):

$$E = (4 \times F \times l^3) / (f \times b \times h^3) \quad (1)$$

where F—applied force, l—length of the microbeam, f—deflection of the microbeam, b—width of the microbeam, and h—thickness of the microbeam.

2.4. Measurement Setup

The measurement setup consisted of a vibration controller Type 2718, a power amplifier Type 2718, a vibration exciter 4809 (10–20 kHz) with a set constant acceleration (1 g), a digital oscilloscope, a laser source (635 nm, 5 mW) with a power supplier, and a photodetector (OP101, Thorlabs) (Figure 2). The electrical output of the harvester was connected to a loading resistance in the range of 10 Ω to 2.4 kΩ to measure output power vs. loading resistance characteristics. Despite collecting the electrical signal from the coil, the optical detection systems (laser and photodetector) were used to determine the resonant frequency of the vibrating microstructure. A charge coupled device (CCD) camera with a video grabber and USB connection (2 megapixels, HDCE-X2, Poland) observed the harvester during operation to monitor the operation of the vibration structure and determine the displacement of the vibrating seismic mass. It captured images at 30 fps. LabView-based home-made software was used to collect the images and analyze for displacement analysis. The optical detection system was calibrated on a certified scale with 100 µm distance marks. It was determined that 91 pixels corresponded to 100 µm length and the accuracy of the measurement technique was ± 2 pixels/ ± 2.6 µm. The software counted the difference in the number of pixels for a non-vibrating mass (initial position) and a mass vibrating at resonant frequency.

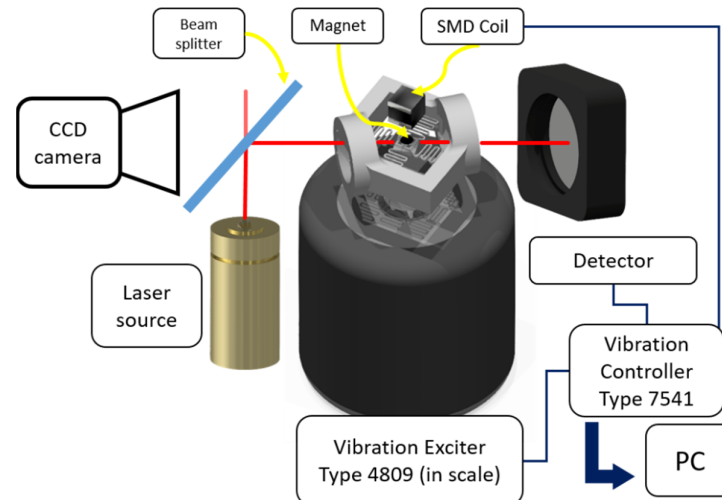


Figure 2. Scheme of the measurement set-up (optical and electrical) applied in the vibrational energy harvester's characterization.

3. Results and Discussion

All the designed harvesters were successfully printed (Figure 3) and tested. The time required for designing and printing the harvesters was less than 4 hours, which is much lower than the time that would have been taken using traditional micromachining methods.

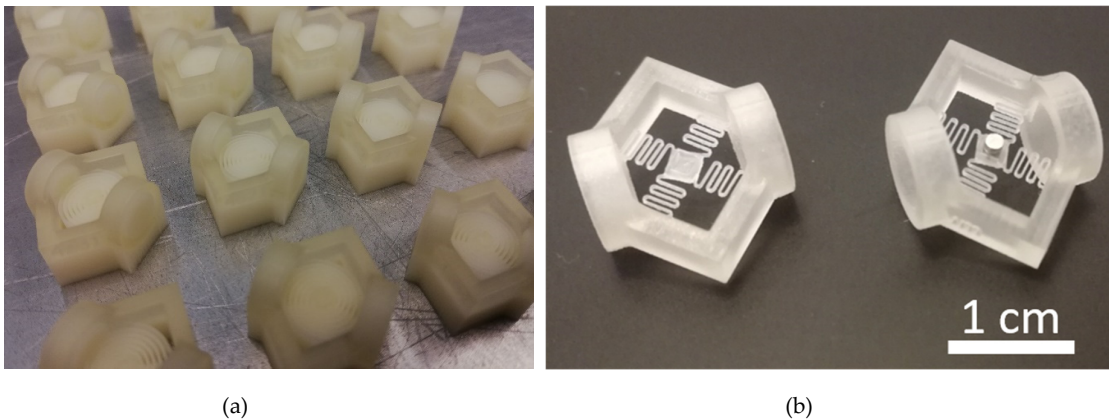


Figure 3. Vibrational 3D-printed MEMS-type energy harvesters: (a) after printing on the printing platform before support material removal, (b) an example of one of the printed structures without and with an assembled miniature magnet.

The calculated Young's modulus values based on deflection vs. force curves (Figure 4), and applied in numerical simulations, were 2240 MPa for 200 m thick and 400 m thick microstructures. Simulations done for the data sheet modulus resulted in a lower resonant frequency, with a difference from 8 Hz to 85 Hz. The resonant values obtained for the calculated Young's modulus were closer to the real values, and the difference between the simulated and measured values was from 3 Hz to 19 Hz. The biggest difference for both the data sheet and the calculated Young's modulus were for thick (1.3 mm) springs. Thus, the Young's modulus declared by the manufacturers can be used to estimate the resonant frequency and the real (measured) value of the modulus can be used to determine the resonant frequency more precisely. Due to the various types of geometry and dimensions of the springs, it was possible to obtain resonant frequencies from 95 Hz to 340 Hz. The harvesters with

circular springs had a narrower bandwidth (6–8 Hz) than the structures with “traditional” springs (20–23 Hz). This is an important observation for the future design of the printed harvesters.

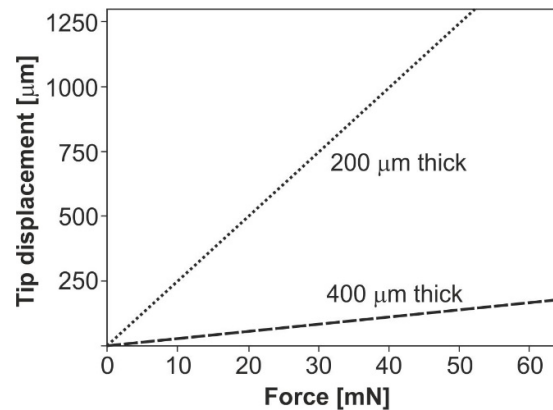


Figure 4. Examples of force vs. tip displacement of the measured 200 m thick and 400 m thick microbeams.

The parameters that influenced the maximal displacement were the geometry of the springs and the number of magnets. Structures with thinner springs operated properly with only one magnet. This was because of a large displacement at resonance and the sticking of the magnet to the coil. As a result, a lower output voltage and power were obtained for these structures. For a structure with two magnets and 400 m thick springs, the maximal measured displacement of the resonating microstructure was around 1.32 mm (Figure 5).

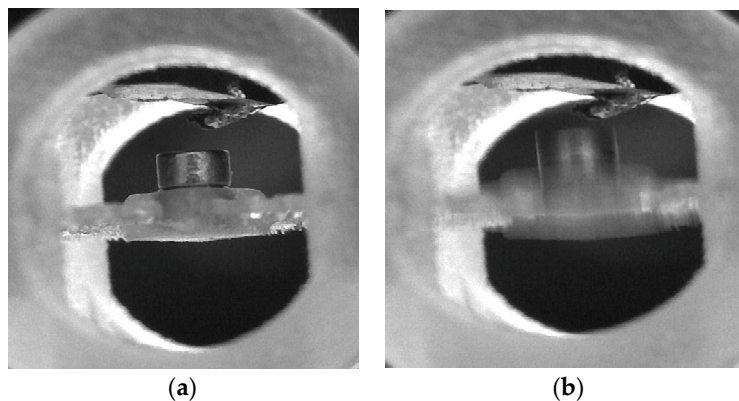


Figure 5. (a) Images captured by the video systems at steady state and (b) during the resonance vibrations with 1.32 mm amplitude.

Thus, at the resonant frequency, the gap between the magnet and the coil was below 0.2 mm. This prevented these two components from sticking together during operation. On the other hand, the smallest amplitude (0.62 mm) was observed for the spiral configuration with $200 \times 200 \text{ m}^2$ springs and one magnet. Thus, the number of magnets (mass of the vibrating structure and the geometry of the magnetic field) and spring geometry (stiffness) significantly influenced the electrical parameters of the harvester. The maximal generated peak-to-peak voltage at resonance was 450 mV. At the optimal loading resistance (Figure 6), this was 23.7 W output power and an energy density of around 400 W/cm^3 for a two-magnet configuration and 400 m thick springs. A lower value of maximal output power (12.6 W) was obtained for a one-magnet configuration and 200 m thick springs but, due to the lower active volume, the power density was higher (almost 600 W/cm^3). This value is in the top range reported for other electromagnetic harvesters, and for the first time it was obtained for a 3D-printed harvester with a total volume below 1 cm^3 . The calculated and measured resonant frequencies, as

well as electrical output parameters, are summarized in Table 1. An important milestone in future work will be the printing of magnets together with the micromechanical structure. Some initial work in this field has been reported in the literature [38–40].

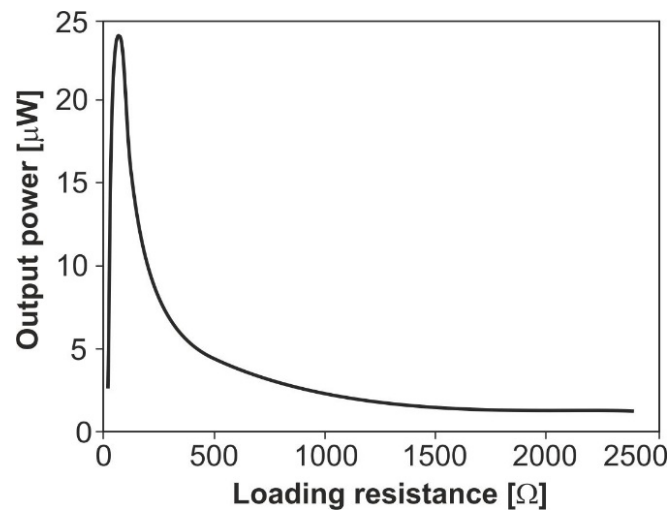






Figure 6. Output power generated by the energy harvester as a function of loading resistance, result for optimal geometry of the 3D-printed microstructure (Table 1).

Table 1. Main parameters of the simulated and 3D-printed MEMS-type electromagnetic energy harvesters.

Visualisation of the Harvester Structure and Number of Magnets	Number of Magnets, Spring Dimensions (Height \times Width [m]), and Rotation Coefficient	Simulated Resonant Frequency [Hz] for Young's Modulus 2240/1463 MPa	Measured Resonant Frequency [Hz]	Maximal Peak-to-Peak Voltage [mV]	Band Width [Hz]	Maximal Output Power [W]	Active Volume [cm ³]	Power Density [W/cm ³]
	Two magnets, 400 \times 400, 1.62	103/92	100	420	6	23.7	0.0596	397
	One magnet, 200 \times 200, 1.62	98/87	95	60	8	7.2	0.0284	253
	One magnet, 200 \times 200	134/117	130	254	23	12.6	0.0212	594
	One magnet, 200 \times 1300	321/255	340	260	20	12.7	0.0486	261

4. Conclusions

The printed prototypes generated up to almost 24 W of power at 1 g acceleration and 61 loading resistance. The mechanical components of the energy harvester were fabricated monolithically using inkjet 3D printing with a 200 m or 400 m thickness typical for MEMS devices. The total volume of the harvesters, including the frame and inductor holder, was below 1 cm³. This was lower than other energy harvesters utilizing 3D printing to print housing or vibrating mechanical structures that have been reported in the literature. The measured resonant frequencies for various geometrical configurations were compared to simulated ones. It was found that the mechanical properties of the building material reported by the manufacturer can be used to estimate resonant frequency. More precise calculations require the real parameters of the mechanical microstructures to be determined. The 3D-printed harvesters were characterized in the measurement setup that enabled both the electrical and optical determination of the resonant frequency. It was possible to measure the output voltage as well as the amplitude of the vibrating microstructure.

Based on the results of this study, it seems that the 3D printing of MEMS-like energy harvesters is possible. Due to the short time from project to real structure, it is possible to experimentally validate real parameters of 3D-printed energy harvesters with various kinds of geometry. The performance of the harvesters we created is sufficient to power low-power sensors and electronic circuits for IoT applications. Further studies will be focused on the integration of printed magnets and multifrequency energy harvesting.

Author Contributions: Conceptualization and supervision R.W.; methodology, design, printing, and measurements B.K.; software for electrical characterization K.Ś.; validation V.C.L.; analysis and vibrational tests Q.S. All authors have read and agreed to the published version of the manuscript.

Funding: The works were realized under NAWA "Academic International Partnerships of Wroclaw University of Science and technology" program by the Polish National Agency for Academic Exchange Program (www.nawa.gov.pl) and National Research Centre (project no. 2019/35/B/ST8/00687).

Conflicts of Interest: The authors declare no conflict of interest.

References

1. Dziuban, J.A. *Bonding in Microsystem Technology*; Springer Science and Business Media LLC: Berlin, Germany 2006.
2. Esashi, M.; Takinami, M.; Wakabayashi, Y.; Minami, K. High-rate directional deep dry etching for bulk silicon micromachining. *J. Micromech. Microeng.* **1995**, *5*, 5–10, doi:10.1088/0960-1317/5/1/002.
3. Shikida, M.; Sato, K.; Tokoro, K.; Uchikawa, D. Differences in anisotropic etching properties of KOH and TMAH solutions. *Sens. Actuator A Phys.* **2000**, *80*, 179–188, doi:10.1016/S0924-4247(99)00264-2.
4. Becker, H.; Gärtner, C. Polymer microfabrication technologies for microfluidic systems. *Anal. Bioanal. Chem.* **2007**, *390*, 89–111, doi:10.1007/s00216-007-1692-2.
5. Sollier, E.; Murray, C.; Maoddi, P.; Di Carlo, D. Rapid prototyping polymers for microfluidic devices and high pressure injections. *Lab Chip* **2011**, *11*, 3752, doi:10.1039/c1lc20514e.
6. Eddings, M.A.; Johnson, M.A.; Gale, B.K. Determining the optimal PDMS–PDMS bonding technique for microfluidic devices. *J. Micromech. Microeng.* **2008**, *18*, 67001, doi:10.1088/0960-1317/18/6/067001.
7. Unger, M.A. Monolithic microfabricated valves and pumps by multilayer soft lithography. *Science* **2000**, *288*, 113–116, doi:10.1126/science.288.5463.113.
8. Golonka, L. Technology and applications of Low Temperature Cofired Ceramic (LTCC) based sensors and microsystems. *Bull. Polish Acad. Sci. Tech. Sci.* **2006**, *54*, 221–231.
9. Bryzek, J. Trillion Sensors Movement in Support of Abundance and Internet of Everything. In Proceedings of the Materials of Sensors Conference, Santa Clara, CA, USA, 6 March 2014.
10. Bhattacharjee, N.; Urrios, A.; Kang, S.; Folch, A. The upcoming 3D-printing revolution in microfluidics. *Lab Chip* **2016**, *16*, 1720–1742, doi:10.1039/c6lc00163g.
11. Waldbaur, A.; Rapp, H.; Länge, K.; Rapp, B.E. Let there be chip—towards rapid prototyping of microfluidic devices: one-step manufacturing processes. *Anal. Methods* **2011**, *3*, 2681, doi:10.1039/c1ay05253e.
12. Bhargava, K.C.; Thompson, B.; Malmstadt, N. Discrete elements for 3D microfluidics. *Proc. Natl. Acad. Sci. USA* **2014**, *111*, 15013–15018, doi:10.1073/pnas.1414764111.

13. Au, A.K.; Lee, W.; Folch, A. Mail-order microfluidics: evaluation of stereolithography for the production of microfluidic devices. *Lab Chip* **2014**, *14*, 1294–301, doi:10.1039/c3lc51360b.
14. O'Neill, P.; Ben Azouz, A.; Vazquez, M.; Liu, J.; Marczak, S.; Slouka, Z.; Chang, H.C.; Diamond, D.; Brabazon, D. Advances in three-dimensional rapid prototyping of microfluidic devices for biological applications. *Biomicrofluidics* **2014**, *8*, 052112, doi:10.1063/1.4898632.
15. Xu, Y.; Wu, X.; Guo, X.; Kong, B.; Zhang, M.; Qian, X.; Mi, S.; Sun, W. The boom in 3D-printed sensor technology. *Sensors* **2017**, *17*, 1166, doi:10.3390/s17051166.
16. Walczak, R. Inkjet 3D printing—towards new micromachining tool for MEMS fabrication. *Bull. Polish Acad. Sci. Tech. Sci.* **2018**, *66*, 179–186.
17. Rogers, C.I.; Qaderi, K.; Woolley, A.T.; Nordin, G.P. 3D printed microfluidic devices with integrated valves. *Biomicrofluid.* **2015**, *9*, 016501, doi:10.1063/1.4905840.
18. Au, A.K.; Bhattacharjee, N.; Horowitz, L.F.; Chang, T.C.; Folch, A. 3D-printed microfluidic automation. *Lab Chip* **2015**, *15*, 1934–1941, doi:10.1039/c5lc00126a.
19. Podwin, A.; Walczak, R.; Dziuban, J.A. A 3D printed membrane-based gas microflow regulator for on-chip cell culture. *Appl. Sci.* **2018**, *8*, 579, doi:10.3390/app8040579.
20. Song, K.; Lee, H.; Cha, Y. A v-shaped actuator utilizing electrostatic force. *Actuators* **2018**, *7*, 30, doi:10.3390/act7020030.
21. Hu, T.; Zhao, Y.-L.; Zhao, Y.; Ren, W. Integration design of a MEMS based fuze. *Sens. Actuator Phys.* **2017**, *268*, 193–200, doi:10.1016/j.sna.2017.09.051.
22. Aspar, G.; Goubault, B.; Lebaigue, O.; Souriau, J.-C.; Simon, G.; Di Cioccio, L.; Brechet, Y. 3D printing as a new packaging approach for MEMS and electronic devices. In Proceedings of the 2017 IEEE 67th Electronic Components and Technology Conference (ECTC), Orlando, FL, USA, 30 May–2 June 2017; pp. 1071–1079.
23. Toshiyoshi, H.; Ju, S.; Honma, H.; Ji, C.-H.; Fujita, H. MEMS vibrational energy harvesters. *Sci. Technol. Adv. Mater.* **2019**, *20*, 124–143, doi:10.1080/14686996.2019.1569828.
24. Torah, R.; Glynne-Jones, P.; Tudor, M.; O'Donnell, T.; Roy, S.; Beeby, S.P. Self-powered autonomous wireless sensor node using vibration energy harvesting. *Meas. Sci. Technol.* **2008**, *19*, 125202, doi:10.1088/0957-0233/19/12/125202.
25. Aktakka, E.E.; Najafi, K. A micro inertial energy harvesting platform with self-supplied power management circuit for autonomous wireless sensor nodes. *IEEE J. Solid-State Circuits* **2014**, *49*, 2017–2029, doi:10.1109/jssc.2014.2331953.
26. Sano, C.; Mitsuya, H.; Ono, S.; Miwa, K.; Toshiyoshi, H.; Fujita, H. Triboelectric energy harvesting with surface-charge-fixed polymer based on ionic liquid. *Sci. Technol. Adv. Mater.* **2018**, *19*, 317–323, doi:10.1080/14686996.2018.1448200.
27. Sakane, Y.; Suzuki, Y.; Kasagi, N. The development of a high-performance perfluorinated polymer electret and its application to micro power generation. *J. Micromech. Microeng.* **2008**, *18*, 104011, doi:10.1088/0960-1317/18/10/104011.
28. Ju, S.; Ji, C.-H. Impact-based piezoelectric vibration energy harvester. *Appl. Energ.* **2018**, *214*, 139–151, doi:10.1016/j.apenergy.2018.01.076.
29. Maharjan, P.; Cho, H.; Rasel, M.; Salauddin; Park, J.Y. A fully enclosed, 3D printed, hybridized nanogenerator with flexible flux concentrator for harvesting diverse human biomechanical energy. *Nano Energ.* **2018**, *53*, 213–224, doi:10.1016/j.nanoen.2018.08.034.
30. Seol, M.-L.; Ivaškevičiūtė-Povilauskienė, R.; Ciappesoni, M.A.; Thompson, F.V.; Moon, D.-I.; Kim, S.J.; Han, J.-W.; Meyyappan, M.; Kim, S.J. All 3D printed energy harvester for autonomous and sustainable resource utilization. *Nano Energ.* **2018**, *52*, 271–278, doi:10.1016/j.nanoen.2018.07.061.
31. Seol, M.-L.; Han, J.-W.; Moon, D.-I.; Yoon, K.J.; Hwang, C.S.; Meyyappan, M. All-printed triboelectric nanogenerator. *Nano Energ.* **2018**, *44*, 82–88, doi:10.1016/j.nanoen.2017.11.067.
32. Hadas, Z.; Zouhar, J.; Singule, V.; Ondrusek, C. Design of energy harvesting generator base on rapid prototyping parts. In Proceedings of the 2008 13th International Power Electronics and Motion Control Conference, Poznan, Poland, 1–3 September 2008; pp. 1665–1669.
33. Rubes, O.; Smilek, J.; Hadas, Z. Development of vibration energy harvester fabricated by rapid prototyping technology. In Proceedings of the 16th International Conference on Mechatronics - Mechatronika 2014, Brno, Czech Republic, 3–5 December 2014; pp. 178–182.
34. Bowers B.; Arnold D. Spherical magnetic generator for bio-motional energy harvesting. In Proceedings of the PowerMEMS 2008 Conference, Sendai, Japan, 9–12 November 2008; pp. 281–284.

35. Constantinou, P.; Roy, S. A 3D printed electromagnetic nonlinear vibration energy harvester. *Smart Mater. Struct.* **2016**, *25*, 95053, doi:10.1088/0964-1726/25/9/095053.
36. Walczak, R.; Adamski, K.; Lizanets, D. Inkjet 3D printed check microvalve. *J. Micromech. Microeng.* **2017**, *27*, 047002, doi:10.1088/1361-6439/aa6152.
37. Walczak, R.; Kawa, B.; Adamski, K. Inkjet 3D printed microfluidic device for growing seed root and stalk mechanical characterization. *Sens. Actuator. Phys.* **2019**, *297*, 111557, doi:10.1016/j.sna.2019.111557.
38. Saleh, E.; Woolliams, P.; Clarke, B.; Gregory, A.; Greedy, S.; Smartt, C.; Wildman, R.D.; Ashcroft, I.; Hague, R.; Dickens, P.; et al. 3D inkjet-printed UV-curable inks for multi-functional electromagnetic applications. *Addit. Manuf.* **2017**, *13*, 143–148, doi:10.1016/j.addma.2016.10.002.
39. Palmero E.; Rial J.; De Vicente J.; Camarero J.; Skarman B.; Vidarsson, H.; Larsson, P.-O.; Bollero, A. Development of permanent magnet MnAlC/polymer composites and flexible filament for bonding and 3D-printing technologies. *Sci. Technol. Adv. Mater.* **2018**, *19*, 465–473.
40. Wang, Z.; Huber, C.; Hu, J.; He, J.; Suess, D.; Wang, S.X. An electrodynamic energy harvester with a 3D printed magnet and optimized topology. *Appl. Phys. Lett.* **2019**, *114*, 013902, doi:10.1063/1.5074123.



© 2020 by the authors. Licensee MDPI, Basel, Switzerland. This article is an open access article distributed under the terms and conditions of the Creative Commons Attribution (CC BY) license (<http://creativecommons.org/licenses/by/4.0/>).